

UC Berkeley

UC Berkeley Previously Published Works

Title

System Identification Study of a 7-Story Full-Scale Building Slice Tested on the UCSD-NEES Shake Table

Permalink

<https://escholarship.org/uc/item/5w94h3vg>

Journal

Journal of Structural Engineering, ASCE, 137(6)

Authors

Moaveni, Babak
He, Xianfei
Conte, Joel P
et al.

Publication Date

2011-06-01

DOI

doi:10.1061/(ASCE)ST.1943-541X.0000300

Peer reviewed

SYSTEM IDENTIFICATION STUDY OF A SEVEN-STORY FULL-SCALE BUILDING SLICE TESTED ON THE UCSD-NEES SHAKE TABLE

**Babak Moaveni¹, A.M. ASCE, Xianfei He², Joel P. Conte³, M. ASCE,
Jose I. Restrepo⁴, M. ASCE, and Marios Panagiotou⁵, M. ASCE**

ABSTRACT

A full-scale seven-story reinforced concrete building slice was tested on the unidirectional UCSD-NEES shake table during the period October 2005 - January 2006. A rectangular wall acted as the main lateral force resisting system of the building slice. The shake table tests were designed to damage the building progressively through four historical earthquake records. The objective of the seismic tests was to validate a new displacement-based design methodology for reinforced concrete shear wall building structures. At several levels of damage, ambient vibration tests and low amplitude white noise base excitations tests were applied to the building which responded as a quasi-linear system with dynamic parameters evolving as a function of structural damage. Six different state-of-the-art system identification algorithms including three output-only and three input-output methods were used to estimate the modal parameters (natural frequencies, damping ratios, and mode shapes) at different damage levels based on the response of the building to ambient as well as white noise base excitations, measured using DC-coupled accelerometers. The modal parameters estimated at various damage

¹ Assistant Professor, Department of Civil and Environmental Engineering, Tufts University, 200 College Avenue, Medford, MA, 02155; E-mail: babak.moaveni@tufts.edu

² Associate Bridge Engineer, AECOM Transportation, 999 Town & Country Road, Orange, CA 92868; E-mail: Daniel.He@aecom.com

³ Professor, Department of Structural Engineering, University of California at San Diego, 9500 Gilman Drive, La Jolla, CA 92093-0085; E-mail: jpconte@ucsd.edu (corresponding author)

⁴ Professor, Department of Structural Engineering, University of California at San Diego, 9500 Gilman Drive, La Jolla, CA 92093-0085; E-mail: jrestrepo@ucsd.edu

⁵ Assistant Professor, Department of Civil and Environmental Engineering, University of California at Berkeley, 747 Davis Hall, Berkeley, CA, 94720-1710; E-mail: panagiotou@ce.berkeley.edu

levels using different system identification methods are compared in order to: (1) validate/cross-check the modal identification results and study the performance of each of these system identification methods, and (2) investigate the sensitivity of the identified modal parameters to actual structural damage. For a given damage level, the modal parameters identified using different methods are found to be in good agreement indicating that these estimated modal parameters are likely to be close to the actual modal parameters of the building specimen.

CE Database subject headings: Building structure; Experimental modal analysis; System identification; Modal parameters; Shake table tests.

INTRODUCTION

In recent years, structural health monitoring has been attracting increasing attention and is of growing importance in the civil engineering research community as a potential tool to develop methods through which structural damage can be identified at the earliest possible stage and the remaining useful life of structures evaluated (damage prognosis). Civil structures may be suddenly damaged due to natural and man-made hazards such as earthquakes, hurricanes, and explosions. Also, material and structural degradation resulting from aging and environmental influences cause progressive structural damage over time. Experimental modal analysis has been developed as a technology for identifying structural dynamic characteristics from recorded structural vibration data. Changes in dynamic characteristics of structures are being used extensively for the purpose of condition assessment and damage identification of structures. Extensive literature reviews on damage identification based on changes in vibration characteristics were provided by Doebling et al. (1996 and 1998) and Sohn et al. (2003). It should be mentioned that the success of damage identification based on experimental modal analysis depends strongly on the accuracy and completeness of the identified structural dynamic properties.

A portion of a reinforced concrete mid-rise residential building, referred to herein as a building slice, was built and tested at full-scale on the UCSD-NEES shake table in the period October 2005 – January 2006. The prototype building represents a type of low-rise cost effective construction for residential buildings proposed in substitution of wood frame construction in densely populated areas of Southern California. The prototype building plan is shown in Figure 1. The lateral force resisting system in the short (transversal) direction of the building consists

primarily of 3.6m long load bearing walls. The building was designed using a displacement based method considering two performance levels: Immediate Occupancy and Life Safety, each anchored at a specified seismic hazard level (Panagiotou and Restrepo 2009a). The considered displacement-based design methodology resulted in significantly smaller earthquake equivalent lateral forces and therefore significantly less longitudinal steel reinforcement in the shear walls than required by current force-based seismic design provisions in the United States. A portion of the building consisting of one shear wall with the surrounding slabs was selected as test specimen. In this portion of the building, unless supported, the slabs are cantilevered from the walls. Thus, to improve the boundary conditions, it was decided to support the slab ends on gravity columns. These seismic tests provided the unique opportunity to observe the dynamic response of a building slice built at full-scale using actual construction practices (e.g., tunnel form construction, joints and lap-splices) at various damage states.

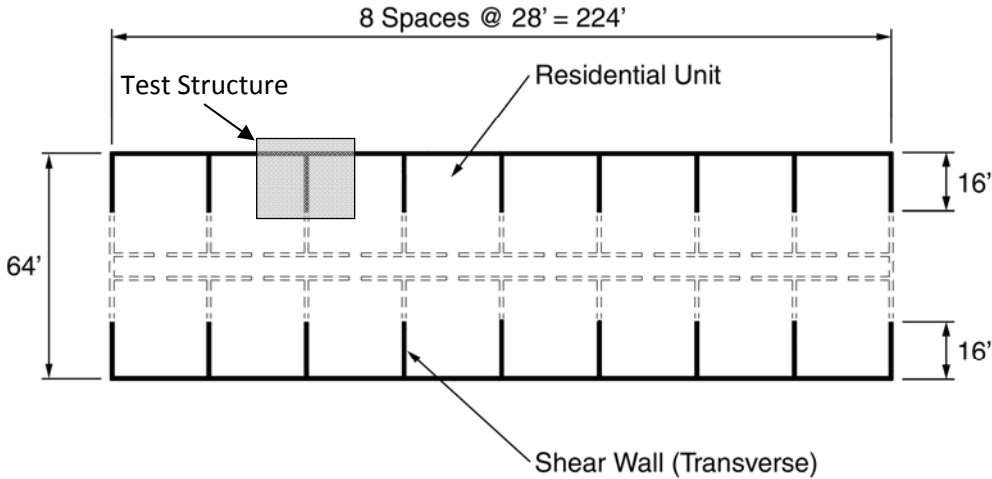


Fig. 1 Plan view of prototype building with cross-section of test structure

Using the measured response of the tested portion of the building to seismic base excitation together with a properly calibrated nonlinear finite element (FE) model, and then extending this calibrated FE model to the whole prototype building structure, the seismic response of the latter can be predicted reliably. The shake table testing of the selected building portion reproduces the actual predominant failure modes (spalling of concrete, lap-splice failures, shear-sliding along construction joints, large curvatures and combined shear-flexural damage patterns) of the prototype building. The building slice was subjected to four historical California earthquake records, including the strong intensity near-fault Sylmar record from the

1994 Northridge earthquake, which induced significant inelastic response and resulting damage to the structure. This project stemmed from the interest in the subject and strong partnership of a construction industry group comprised mainly of contractors, construction product suppliers and practicing structural engineers mostly from Southern California. The building specimen responded very satisfactorily to the earthquake ground motions reproduced by the shake table and met all performance objectives. The effects on the experimental response of the interaction between the walls, the slabs and the gravity system as well as the effect of higher modes were found to be very significant (Panagiotou and Restrepo 2009a; Panagiotou et al. 2009b).

The shake table tests were designed to damage the building progressively through four historical earthquake ground motions. At various levels of damage, ambient vibration tests were performed and low amplitude white noise base excitations were applied to the building through the shake table. During these ambient vibration and white noise base excitation tests, the building responded as a quasi-linear system with dynamic parameters evolving as a function of structural damage. Six different state-of-the-art system identification methods, consisting of three input-output and three output-only methods, were applied to the dynamic response of the building measured using DC-coupled accelerometers to estimate modal parameters (natural frequencies, damping ratios and mode shapes) of the building in its undamaged (baseline) and various damage states. The system identification methods used are: (1) Multiple-reference Natural Excitation Technique combined with Eigensystem Realization Algorithm (MNExT-ERA) (James et al. 1993); (2) Data-driven Stochastic Subspace Identification (SSI-DATA) (Van Overschee and de Moor 1996); (3) Enhanced Frequency Domain Decomposition (EFDD) (Brinker et al. 2001); (4) Deterministic-Stochastic Subspace Identification (DSI) (Van Overschee and de Moor 1996); (5) Observer/Kalman filter Identification combined with ERA (OKID-ERA) (Phan et al. 1992); and (6) General Realization Algorithm (GRA) (de Callafon et al. 2008). The first three algorithms are based on output-only data (from ambient vibration and white noise base excitation tests) while the latter three require measured input and output data (from the white noise base excitation tests). The three output-only system identification methods used here were successfully applied by the authors to dynamic field test data from the Alfred Zampa Memorial Bridge (He et al. 2009).

Different system identification methods provide modal parameter estimators with different intra-method and inter-methods statistical properties (bias, variance, co-variance), which

depend on the amplitude and frequency content of the input excitation, the degree of violation of the hypotheses based on which these methods were developed (e.g., linear system, broad-band excitation, response stationarity), etc. In a previous study, the authors have investigated the effects of such factors on the performance of the three output-only system identification methods used here based on the dynamic response of the seven-story reinforced concrete building slice simulated using a three-dimensional nonlinear finite element model (Moaveni et al. 2007). It was found that for all three methods, the estimation bias and variability for the natural frequencies and mode shapes are very small and the estimation uncertainty of the damping ratios is significantly higher than that of the natural frequencies and mode shapes.

TEST SPECIMEN, TEST SETUP AND DYNAMIC EXPERIMENTS

Seven-Story Reinforced Concrete Building Slice

The test structure which represents a slice of a full-scale reinforced concrete building consists of a main wall (web wall), a back wall (flange wall) perpendicular to the main wall for transversal stability, a concrete slab at each floor level, an auxiliary post-tensioned column to provide torsional stability, and four gravity columns to transfer the weight of the slabs to the shake table. Slotted slab connections located between the web and flange walls at floor levels minimize the moment transfer between the two walls, while allowing the transfer of the in-plane diaphragm forces. Figure 2 shows the test structure mounted on the shake table. More details about the test structure can be found in Panagiotou and Restrepo (2009a) and Panagiotou et al. (2009b).

Instrumentation Layout

The test structure was instrumented with a dense array of DC-coupled accelerometers, strain gages, potentiometers, and linear variable displacement transducers (LVDTs), all sampling data simultaneously using a nine-node distributed data acquisition system. The accelerometer array consisted of 14 channels of acceleration measurements on the foundation/pedestal of the test structure, 106 on the floor slabs and the web wall, 17 channels on the reaction block of the shake table and one tri-axial accelerometer on the surrounding ground surface (free field), resulting in a total of 140 acceleration channels. A set of 54 LVDT were installed along both

edges (east and west) of the web wall and 8 potentiometers were installed over the first two stories of the web wall. A total of 231 strain gages were distributed on the test specimen as follows: 143 on the steel reinforcement of the web wall, 64 on the steel reinforcement of the flange wall, 16 on the gravity columns and 8 on the steel braces connecting the slabs to the post-tensioned column. In addition, the displacement responses of 6 selected points on the structure (3 on the top floor slab, 2 on the flange wall and 1 on the shake table platen) were measured in three dimensions using 6 global positioning system (GPS) sensors. The technical characteristics of the accelerometers are: MEMS-Piezoresistive MSI model 3140, amplitude range: +/-5g, frequency range (min): 0-300Hz, voltage sensitivity: 400mV/g. The data acquisition system used consisted of nine distributed 16-bit resolution National Instruments PXI chassis. Each chassis had eight SCXI 1520 modules which were individually configured to handle eight channels of strain gages, accelerometers, relative displacement, and/or pressure transducers.



Fig. 2 Test structure

In this study, measured response data from 28 longitudinal acceleration channels (three on each floor slab and one on the web wall at mid-height of each story) were used to identify the

modal parameters of the test structure. It should be mentioned that the output-only methods used here were also applied to the strain measurement data obtained from the LVDTs located along both edges of the web wall of the structure and the corresponding system identification results are reported in Moaveni (2007). Figure 3 shows the Fourier Amplitude Spectra (FAS) of two filtered (between 0.5Hz and 25Hz using a Finite Impulse Response filter of order 1024) acceleration time histories recorded at floor levels 1 and 7 during a 0.03g root-mean-square (RMS) acceleration white noise base excitation test (left column) and an ambient vibration test (right column) performed on the structure in its undamaged state. From this figure, it is observed that: (1) the FAS plots are very jagged/noisy which may be due to rattling of loose connections especially from the slackness between the threaded rod and the nut in the gravity columns (1.5mm of slackness) when they go from tension to compression or vice versa as well as the slackness at both ends of the steel braces connecting the slabs to the post-tensioned column; (2) the first longitudinal vibration mode has a predominant contribution to the total response, especially at the higher floors, which renders the identification of higher (than the first longitudinal) vibration modes more difficult; and (3) the FAS of the acceleration response histories at the first floor appear to have a drop in amplitude at around 11.5 Hz which is due to the application of a notch filter in the control loop of the table to reduce the effects of the oil column resonance. Mechanical characteristics of the shake table are available in Ozcelik (2008).

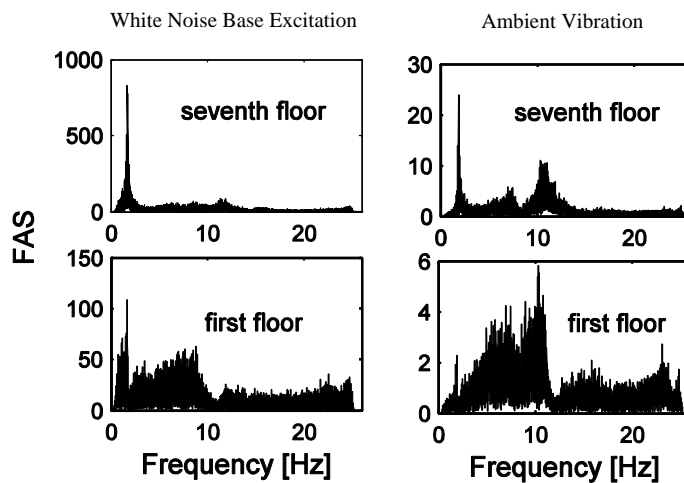


Fig. 3 Fourier Amplitude Spectra of acceleration response measurements at the first and seventh (roof) floors due to white noise base excitation (left) and ambient excitation (right)

It is worth noting that all the target base excitation signals (white noise base acceleration and earthquake ground acceleration records) reproduced on the shake-table were distorted due to

the limitations of the shake-table controller and the table-structure interaction. However, the reproduced base excitations were measured on top of the shake-table platen and used in the input-output system identification methods. The input signal distortion are shown to have little effect on the output-only system identification results as they are found in very good agreement with those obtained from the input-output methods. In the case of the output-only methods, the effects of table-structure interaction were reduced by using horizontal accelerations relative to the base of the specimen. Another effect of table-structure interaction is the rocking of the structure at its base, which is made of two components: (1) bending of the shake table platen and vertical deformations of (i) the hydraulic bearings, (ii) the foundation, and (iii) the surrounding soil; and (2) localized rotation manifested at the base of the web wall caused by strain penetration of the longitudinal reinforcing bars into the foundation in which they are anchored and partial debonding (bond-slip) of these bars. Although the second component of the rocking of the wall contributes up to 7 percent of the peak measured roof relative horizontal displacement for earthquake tests EQ2 and EQ3 (Panagiotou et al. 2009b), it has a much lower (negligible) relative contribution for lower amplitude ambient and white noise base excitations. The small (i.e., few percent relative contribution) first component of the rocking of the wall could not be removed from the measured data before performing system identification due to the low signal-to-noise ratio of the vertical accelerometers measuring the rocking of the shake table platen at the base of the specimen.

Dynamic Tests Performed

A sequence of dynamic tests (68 tests in total) was applied to the test structure during the period October 2005 - January 2006 including ambient vibration tests, free vibration tests, and forced vibration tests (white noise and seismic base excitations) using the UCSD-NEES shake table. The structure was damaged progressively through four historical earthquake ground motions and the modal parameters of the structure were identified at various damage states using different state-of-the-art system identification methods and different dynamic test data.

The four historical earthquake records applied to the test structure were: (1) longitudinal component of the 1971 San Fernando earthquake ($M_w = 6.6$) recorded at the Van Nuys station (EQ1), (2) transversal component of the 1971 San Fernando earthquake recorded at the Van Nuys station (EQ2), (3) longitudinal component of the 1994 Northridge earthquake ($M_w = 6.7$)

recorded at the Oxnard Boulevard station in Woodland Hill (EQ3), and (4) 360 degree component of the 1994 Northridge earthquake recorded at the Sylmar station (EQ4). The input white noise base excitation consisted of two 8 minute long realizations of a banded white noise (0.25-25Hz) process with root-mean-square (RMS) amplitudes of 0.03g and 0.05g, respectively. Table 1 reports the dynamic tests used in the present study on system identification of this seven-story building structure at various damage states.

Table 1. Dynamic tests used in this study
(WN: white noise base excitation test and AV: ambient vibration test)

Test No.	Date	Test Description	Damage State
39	11/21/2005	8min WN (0.03g) + 3min AV	S0
40	“	EQ1	
41	“	8min WN (0.03g) + 3min AV	S1
42	“	8min WN (0.05g)	S1
43	“	EQ2	
46	11/22/2005	8min WN (0.03g) + 3min AV	S2
47	“	8min WN (0.05g)	S2
48	“	EQ3	
49	“	8min WN (0.03g) + 3min AV	S3.1
50	“	8min WN (0.05g)	S3.1
61	1/14/2006	8min WN (0.03g) + 3min AV	S3.2
62	“	EQ4	
64	1/14/2006	8min WN (0.03g) + 3min AV	S4
65	“	8min WN (0.05g)	S4

The use of four earthquake input motions with distinct features and intensities allowed monitoring of the development of different damage states in the building specimen. Overall, the response was slightly nonlinear for EQ1, moderately nonlinear for the “medium” intensity input motions EQ2 and EQ3, and highly nonlinear for input motion EQ4. During test EQ1, limited yielding occurred in the longitudinal reinforcing steel of the web wall. After this test, cracking of the web wall was widespread and visible up to the fourth floor. During tests EQ2 and EQ3, moderate yielding occurred in the web wall longitudinal reinforcement. Lastly, during test EQ4, localized plasticity developed at the first floor of the web wall. The roof drift ratio, defined as the ratio between the maximum lateral displacement at the roof level of the building and the height of the roof relative to the base of the building, was measured as 0.28%, 0.75%, 0.83%, and 2.1%

in tests EQ1 to EQ4, respectively. The maximum tensile strain in the longitudinal reinforcing steel was measured close to the base of the wall as 0.61%, 1.73%, 1.78%, and 2.85% in tests EQ1 to EQ4, respectively (yield strain of reinforcing steel = 0.22%). In-depth information about the behavior of this building specimen during the seismic tests EQ1 through EQ4 can be found elsewhere (Panagiotou et al. 2009b).

REVIEW OF SYSTEM IDENTIFICATION METHODS USED

Six state-of-the-art linear system identification methods were applied to estimate the modal parameters of the test structure at various damage states. These methods are: (1) Multiple-reference Natural Excitation Technique used in combination with the Eigensystem Realization Algorithm (MNExT-ERA), (2) Data-driven Stochastic Subspace Identification (SSI-DATA), (3) Enhanced Frequency Domain Decomposition (EFDD), (4) Deterministic-stochastic Subspace Identification (DSI), (5) Observer/Kalman filter Identification combined with ERA (OKID-ERA), and (6) General Realization Algorithm (GRA). These methods are all based on linear system theory. If applied to nonlinear response measurements (i.e., data recorded from nonlinear systems), the identified modal parameters are to be interpreted as effective/equivalent modal parameters or modal parameters of an equivalent linear system. It is important to mention that in the linear dynamic models identified using these methods, linear viscous damping is the only source of energy dissipation. Therefore, the effects of other actual sources of energy dissipation such as friction, yielding, and impact are lumped into the equivalent viscous damping. An actual reinforced concrete structure is nonlinear from the onset of loading, i.e., even when subjected to low amplitude excitation, and is also characterized by a number of energy dissipation mechanisms. It then follows that the modal identification results obtained using these methods suffer modeling errors in addition to estimation errors.

The six system identification methods used in this study are briefly reviewed in this section. The measured acceleration responses were sampled at 240Hz resulting in a Nyquist frequency of 120Hz, which is much higher than the modal frequencies of interest in this study (< 25Hz). Before applying the above mentioned system identification methods to the measured data, all the absolute acceleration time histories were band-pass filtered between 0.5Hz and 25Hz using a high order (1024) Finite Impulse Response (FIR) filter. Furthermore, the absolute

horizontal acceleration measurements from the white noise base excitation tests were converted to relative acceleration by subtracting the base/table horizontal acceleration.

Output-Only System Identification Methods

The first three algorithms are based on output-only data (i.e., no information about the input excitation is used) and applied to the measured vibration data from both the ambient vibration and white noise base excitation tests. These methods are based on the assumption of a broadband (ideally white noise) input excitation. The more this assumption is violated, the larger the estimation errors of the identified modal parameters are. The three output-only system identification methods used in this study are briefly described below.

Multiple-reference Natural Excitation Technique Combined with Eigensystem Realization Algorithm (MNE_xT-ERA)

The basic principle behind the Natural Excitation Technique (NExT) is that the theoretical cross-correlation function between two response measurements made along two degrees of freedom collected from an ambient (broad-band) excited structure has the same analytical form as the free vibration response of the structure (James et al. 1993). Once an estimation of the response cross-correlation vector is obtained for a given reference channel, the ERA method (Juang and Pappa 1985) can be used to extract the modal parameters. A key issue in the application of NExT is to select the reference channel so as to avoid missing modes in the identification process due to the proximity of the reference channel to a modal node. In the MNE_xT, instead of using a single reference response channel as in the NExT, a vector of reference channels (three reference channels in this study) is used to obtain an output cross-correlation matrix (He et al. 2009). The response cross-correlation functions were estimated through inverse Fourier transformation of the corresponding cross-spectral density (CSD) functions. CSD function estimation was based on Welch-Bartlett's method using Hanning windows of length 116 seconds (27,840 samples) for white noise base excitation and 15 seconds (3,600 samples) for ambient vibration, with 50 percent of window overlap. The estimated cross-correlation functions were then down-sampled to 80Hz in order to improve the computational efficiency of the identification algorithm and, finally, they were used to form Hankel matrices of size $(28 \times 150) \times 150$ (28 output channels, 150 block rows and 150 columns) for applying ERA in

the second stage of the modal identification. After down-sampling, the Nyquist frequency (40Hz) remains higher than the natural frequencies of the vibration modes of interest (25Hz, see Figure 3). The identified natural frequencies and damping ratios of the vibration modes contributing significantly to the response (longitudinal, torsional and coupled longitudinal-torsional modes) are reported in Table 2 for the ambient vibration data and in Tables 3 and 4 for the white noise base excitation response (output) data.

Table 2. Natural frequencies and damping ratios identified based on ambient vibration test data

State / Test No.	System ID Method	Natural Frequency [Hz]					Damping Ratio [%]				
		1 st -L mode	1 st -T mode	1 st -L-T mode	2 nd -L mode	3 rd -L mode	1 st -L mode	1 st -T mode	1 st -L-T mode	2 nd -L mode	3 rd -L mode
S0 / Test 39	MNExT-ERA	1.92	-	7.05	10.49	24.79	3	-	5	2.5	0.9
	SSI	1.89	-	7.07	10.53	24.58	1.9	-	4.1	2.4	0.4
	EFDD	1.9	-	7.22	10.93	24.76	1.3	-	0.2	0.2	0.2
S1 / Test 41	MNExT-ERA	1.86	-	6.62	10.27	22.98	1.2	-	3.5	3.4	2.4
	SSI	1.86	-	6.81	10.24	24.3	2	-	2.9	2.6	0.6
	EFDD	1.88	-	6.62	10.33	23.45	0.5	-	0.3	0.6	0
S2 / Test 46	MNExT-ERA	1.67	2.04	7.58	10.34	22.78	2.1	1	3.4	1.6	1.4
	SSI	1.67	2.05	7.58	10.16	22.6	1.3	0.9	3	1.4	0.9
	EFDD	1.66	2.07	7.54	10.14	22.8	2.5	1.4	0.2	0.2	0.2
S3.1 / Test 49	MNExT-ERA	1.46	-	7.21	10.06	21.89	3.4	-	2.7	1.4	1.7
	SSI	1.46	1.91	7.18	9.28	21.6	2.9	1.4	2.1	1.1	1.6
	EFDD	1.44	-	7.03	9.28	21.81	0.8	-	0.1	0.2	0.1
S3.2 / Test 61	MNExT-ERA	1.58	1.95	-	8.39	22.97	1.5	0.5	-	2.3	1.2
	SSI	1.58	1.95	-	8.52	22.83	1.4	1.1	-	2.8	1
	EFDD	1.58	1.95	-	8.44	22.87	2	1.1	-	0.3	0.1
S4 / Test 64	MNExT-ERA	1.02	-	-	5.68	15.04	1.2	-	-	2.4	0.8
	SSI	1.02	-	-	5.69	15.05	1	-	-	1.8	1.3
	EFDD	1	-	-	5.74	15.1	1.7	-	-	0.2	0.1

Data-Driven Stochastic Subspace Identification (SSI-DATA)

The SSI-DATA method determines the system model in state-space based on the output-only measurements directly (Van Overschee and de Moor 1996). One advantage of this method compared to two-stage time-domain system identification methods such as covariance-driven stochastic subspace identification and NExT-ERA is that it does not require any pre-processing

of the data to calculate auto/cross-correlation functions or spectra of output measurements. This method involves numerical techniques such as QR factorization, singular value decomposition (SVD) and least squares. In the implementation of SSI-DATA, the filtered acceleration data were down-sampled to 80Hz in order to increase the computational efficiency of the identification algorithm. For each dynamic test, an output Hankel matrix was formed including 35 block rows with 28 rows per block (28 longitudinal acceleration channels) for both white noise and ambient vibration tests, with 24,931 columns for white noise tests and 14,331 columns for ambient vibration tests. It should be noted that the durations of the ambient vibration tests (3 minutes) and white noise base excitation tests (8 minutes) are different (see Table 1). Therefore, different number of columns were used in forming the corresponding Hankel matrices. The natural frequencies and damping ratios of the vibration modes contributing significantly to the response and identified using SSI-DATA are reported in Table 2 for the ambient vibration data and in Tables 3 and 4 for the white noise base excitation response (output) data.

Table 3. Natural frequencies and damping ratios identified based on 0.03g RMS white noise base excitation test data

State / Test No.	System ID Method	Natural Frequency [Hz]					Damping Ratio [%]				
		1 st -L mode	1 st -T mode	1 st -L-T mode	2 nd -L mode	3 rd -L mode	1 st -L mode	1 st -T mode	1 st -L-T mode	2 nd -L mode	3 rd -L mode
S0 / Test 39	MNE _x T-ERA	1.71	2.35	8.64	11.49	24.67	3.1	-1.1	5.4	4.8	1.3
	SSI	1.66	-	8.67	11.65	24.61	2.2	-	3.6	4.4	0.2
	EFDD	1.72	-	8.52	11.88	24.64	2.6	-	1.3	0.5	0.4
	DSI	1.72	1.8	9.03	10.7	24.55	2.2	3.5	4.2	4.5	0.5
	OKID-ERA	1.7	-	8.95	10.78	25.06	1.7	-	0.1	1.5	1.4
	GRA	1.71	-	9.05	11.05	24.31	2.1	-	1.8	1.8	0.5
S1 / Test 41	MNE _x T-ERA	1.54	2.34	8.51	11.35	24.65	4.3	1.1	4.7	7.7	0.9
	SSI	1.51	1.73	8.37	11.25	24.57	2.4	4	4.9	3.3	0.2
	EFDD	1.49	-	8.17	11.33	24.56	3.3	-	1	0.4	0.2
	DSI	1.57	1.78	8.76	10.67	24.42	3.1	2.9	3.9	3.2	0.3
	OKID-ERA	1.6	-	-	10.75	24.57	3.8	-	-	0.3	1.9
	GRA	1.54	-	8.65	10.98	24.28	2	-	1.1	1.7	0.2
S2 / Test 46	MNE _x T-ERA	1.22	-	7.42	10.88	21.26	3.4	-	6	0.3	3.9
	SSI	1.25	-	7.26	11.1	22.82	4.5	-	4.2	4.9	2
	EFDD	1.29	-	7.43	10.75	21.08	5.2	-	0.9	0.3	0.2
	DSI	1.27	2.02	7.67	10.23	21.56	3.5	11.6	6.7	4.8	2.7
	OKID-ERA	1.24	-	7.86	10.93	21.08	2.8	-	-0.3	1.7	2.9
	GRA	1.24	-	7.6	11.11	21.59	3	-	4	2.9	0.5

S3.1 / Test 49	MNEXT-ERA	1.11	-	7.01	10.24	19.77	3.5	-	8.6	7	5.6
	SSI	1.13	2.13	7.14	9.87	20.4	3.9	10.7	3.7	1.9	2.3
	EFDD	1.13	-	7.07	10.06	19.83	4	-	0.3	0.2	0.1
	DSI	1.14	2.2	7.2	-	20.42	3.3	13.3	4.9	-	2.7
	OKID-ERA	1.17	-	7.15	10.47	20.4	5.6	-	0.2	1.8	1.1
	GRA	1.14	-	7.32	9.77	19.68	3.9	-	4.3	1.6	0.5
S3.2 / Test 61	MNEXT-ERA	1.18	2.37	-	11	21.32	5	0	-	6	5.7
	SSI	1.2	2.62	-	10.89	21.04	3.5	4.3	-	5.4	2
	EFDD	1.23	-	-	10.41	20.68	4.6	-	-	0.4	0.1
	DSI	1.22	-	-	-	21.47	3.6	-	-	-	2.7
	OKID-ERA	1.2	-	-	-	20.47	2.8	-	-	-	2.8
	GRA	1.2	-	-	10.45	21.11	3.5	-	-	2	0.3
S4 / Test 64	MNEXT-ERA	0.83	-	-	4.68	13.24	3.3	-	-	7.6	0.4
	SSI	0.85	-	-	4.68	14.02	5.6	-	-	5.5	2.9
	EFDD	0.86	-	-	4.71	13.81	3.8	-	-	0.4	0.2
	DSI	0.85	-	-	4.72	13.31	3.6	-	-	6.1	4.8
	OKID-ERA	0.87	-	-	4.79	14.69	2.9	-	-	3.6	0
	GRA	0.88	-	-	4.81	13.29	5.5	-	-	3.8	0.9

Enhanced Frequency Domain Decomposition (EFDD)

The Frequency Domain Decomposition (FDD) method, a non-parametric frequency-domain approach, is an extension of the basic frequency domain approach also referred to as peak picking technique. According to the FDD technique, the modal parameters are estimated through SVD of the CSD matrix performed at all discrete frequencies. Through this SVD, CSD functions are decomposed into single-degree-of-freedom (SDOF) CSD functions, each corresponding to a single vibration mode of the dynamic system. Considering a lightly damped system, the contribution of different vibration modes at a particular frequency is limited to a small number (usually 1 or 2). In the EFDD method (Brincker et al. 2001), the natural frequency and damping ratio of a vibration mode are identified from the SDOF CSD function corresponding to that mode. In doing so, the SDOF CSD function is taken back to the time domain by inverse Fourier transformation, and the frequency and damping ratio of the mode considered are estimated from the zero-crossing times and the logarithmic decrement, respectively, of the corresponding SDOF auto-correlation function. In applying the EFDD method, the measured acceleration data were down-sampled to 80Hz and then the CSD functions were estimated based on Welch-Bartlett's method using Hanning window with 50 percent

overlap. After estimating the CSD functions, the (28×28) response CSD matrix was singular value decomposed at each discrete frequency. The modal parameters identified using this method are given in Table 2 based on the ambient vibration data and in Tables 3 and 4 based on the white noise base excitation response (output) data.

Table 4. Natural frequencies and damping ratios identified based on 0.05g RMS white noise base excitation test data

State / Test No.	System ID Method	Natural Frequency [Hz]			Damping Ratio [%]		
		1 st -L mode	2 nd -L mode	3 rd -L mode	1 st -L mode	2 nd -L mode	3 rd -L mode
S1 / Test 41	MNExT-ERA	1.39	10.79	24.26	4.1	7.6	2.2
	SSI	1.4	11.38	24.29	3.6	3.5	1.4
	EFDD	1.4	10.97	24.39	2.8	3.3	1.1
S2 / Test 46	MNExT-ERA	1.12	10.41	20.29	5.3	7.7	4.3
	SSI	1.14	10.24	22.46	3.5	2.4	1.1
	EFDD	1.12	10.09	20.09	4.3	3.6	1.6
S3.1 / Test 49	MNExT-ERA	1.05	10.22	19.12	4.4	6.8	7.9
	SSI	1.06	10.23	18.98	3.7	3.3	4.7
	EFDD	1.04	10.1	18.88	4.4	6.3	1.1
S4 / Test 64	MNExT-ERA	0.8	4.62	13.03	3.4	9.7	13.3
	SSI	0.81	4.52	13.67	4.6	6.1	8.4
	EFDD	0.82	4.62	13.29	3.1	3.1	2.3

Input-Output System Identification Methods

The three input-output system identification methods are applied only to the 0.03g RMS white noise base excitation test data, which includes the measurement of the input base excitation. These methods are briefly described below.

Deterministic-Stochastic Subspace Identification (DSI)

The deterministic-stochastic state-space model for linear time-invariant systems can be written as

$$\begin{cases} \mathbf{x}(k+1) = \mathbf{A}\mathbf{x}(k) + \mathbf{B}\mathbf{u}(k) + \mathbf{w}(k) \\ \mathbf{y}(k) = \mathbf{C}\mathbf{x}(k) + \mathbf{D}\mathbf{u}(k) + \mathbf{v}(k) \end{cases} \quad (1)$$

where \mathbf{A} , \mathbf{B} , \mathbf{C} and \mathbf{D} refer to the state-space matrices, $\mathbf{u}(k)$ and $\mathbf{y}(k)$ denote the input and output vectors, respectively, and $\mathbf{x}(k)$ is the state vector. In the deterministic-stochastic model, the process noise $\mathbf{w}(k)$ represents disturbances (small unmeasured excitations) and modeling inaccuracies, while the measurement noise $\mathbf{v}(k)$, models the sensor inaccuracies. However, in the SSI-DATA, both noise terms (\mathbf{w} and \mathbf{v}) also include implicitly the input excitation since it is impossible to distinguish the input information from the noise terms. Considering the following two assumptions: (1) the deterministic input $\mathbf{u}(k)$ is uncorrelated with both the process noise $\mathbf{w}(k)$ and the measurement noise $\mathbf{v}(k)$, and (2) both noise terms are not identically zero, a robust identification algorithm was developed by Van Overschee and de Moor (1996) in order to identify the state-space matrices in the combined deterministic-stochastic system. Similar to SSI-DATA, numerical techniques such as QR factorization, SVD, and least squares are used in this method. In the application of this method, the measured input (shake table acceleration) and the relative horizontal acceleration response data were down-sampled to 80Hz. For each dynamic test, an input-output Hankel matrix was formed including 35 block rows with 29 rows each (1 input and 28 output channels) and 24,931 columns using the down-sampled data. The natural frequencies and damping ratios of the first five significant vibration modes (first three longitudinal, first torsional and first coupled longitudinal-torsional) identified from the 0.03g RMS white noise base excitation test data are reported in Table 3.

Observer/Kalman Filter Identification Combined with ERA (OKID-ERA)

In this method, developed by Phan et al. (1992), the system input-output relationship is expressed in terms of an observer, which is made asymptotically stable by an embedded eigenvalue assignment procedure. The prescribed eigenvalues for the observer may be real, complex, mixed real and complex, or zero (i.e., deadbeat observer). In this formulation, the Markov parameters of the observer are identified from input-output data. The Markov parameters of the actual system are then calculated from those of the observer and then used to obtain a state-space model of the system by ERA. The method performs quite well for finite-dimensional systems under the following conditions: (1) the input-output data time histories are sufficiently long, (2) the noise is white and zero-mean, and (3) the noise-to-signal ratio is small (Lus et al. 2002). This approach is practical, especially for single input systems as in the case of structures subjected to single component base excitation. In the application of OKID-ERA, the filtered and then

detrended (by subtracting the mean value) relative acceleration responses from the white noise base excitation tests were down-sampled to 60Hz. An output matrix $\mathbf{Y} = [\mathbf{y}(0) \ \dots \ \mathbf{y}(p) \ \dots \ \mathbf{y}(l-1)]$ of size (28×1000) (i.e., $l = 1000$) and an input-output matrix \mathbf{V} of size (7251×1000) (i.e., $p = 250$) are formed based on inputs $u(k)$, outputs $\mathbf{y}(k)$, and

input-output vectors $\mathbf{v}(k) = \begin{bmatrix} u(k) \\ \mathbf{y}(k) \end{bmatrix}$ as:

$$\mathbf{V} = \begin{bmatrix} u(0) & u(1) & \dots & u(p) & \dots & u(l-1) \\ \mathbf{0} & \mathbf{v}(0) & \dots & \mathbf{v}(p-1) & \dots & \mathbf{v}(l-2) \\ \vdots & \vdots & \ddots & \vdots & \ddots & \vdots \\ \mathbf{0} & \mathbf{0} & \dots & \mathbf{v}(0) & \dots & \mathbf{v}(l-p-1) \end{bmatrix} \quad (2)$$

The Markov parameters of the observer system \mathbf{M} are estimated as $\mathbf{M} = \mathbf{Y}\mathbf{V}^\dagger$, where \mathbf{V}^\dagger is the pseudo-inverse of \mathbf{V} . Once the true system's Markov parameters are retrieved from the observer's Markov parameters, the ERA is used for estimation of the modal parameters which are reported in Table 3.

General Realization Algorithm (GRA)

GRA (de Callafon et al. 2008) is a system realization algorithm to identify modal parameters of linear dynamic systems based on general input-output data. This algorithm is an extension of ERA. While ERA is based on SVD of a Hankel matrix constructed from impulse response or free vibration response data, GRA is based on SVD of a weighted Hankel matrix, where the weighting is defined by the loading. Using GRA, the state-space matrices are estimated in a two-step process consisting of a state reconstruction followed by a least squares optimization yielding a minimum prediction error for the response. In the application of GRA, a weighted Hankel matrix of size $(28 \times 50) \times 7000$ is formed based on the input-output data. After performing an SVD of this weighted Hankel matrix, a state-space realization of the system is estimated from which the modal parameters are extracted. The natural frequencies and damping ratios identified using GRA are reported in Table 3.

MODAL IDENTIFICATION RESULTS

Modal parameters of the test structure were identified using the system identification methods outlined above based on output-only (for the first three methods) and input-output (for the last three methods) data measured from low amplitude dynamic tests (i.e., ambient vibration tests, 0.03g and 0.05g RMS white noise base excitation tests) performed at various damage states (S0, S1, S2, S3.1, S3.2, and S4). Damage state S0 is defined as the undamaged (baseline) state of the structure before its exposure to the first seismic excitation (EQ1), while damage states S1, S2, S3 and S4 correspond to the state of the structure after exposure to the first (EQ1), second (EQ2), third (EQ3), and fourth (EQ4) seismic excitations, respectively (see Table 1). Damage state S0 does not correspond to the uncracked state of the structure, since the structure had already been subjected to low-amplitude white noise base excitations (0.02-0.03g RMS) for the purposes of checking the instrumentation and data acquisition system and tuning the shaking table controller. It is important to mention that during damage state S3, the bracing system between the slabs of the test specimen and the post-tensioned column was modified (strengthened and stiffened). Therefore, damage state S3 is subdivided into state S3.1 (before modification of the braces) and state S3.2 (after modification of the braces). The identified modal parameters are presented and discussed in the following three subsections based on the type of excitation (ambient, 0.03g and 0.05g RMS white noise base excitations).

Modal Parameters Identified Based on Ambient Vibration Test Data

The modal parameters identified based on acceleration data from ambient vibration tests are discussed in this section. Figure 4 shows in polar plots the complex-valued mode shapes of the five most significantly excited modes of the test structure identified using SSI-DATA based on data from Test 46 (damage state S2). The real parts of these mode shapes are displayed in Figure 5. The five most significant vibration modes identified at this damage state consist of the first three longitudinal (1st-L, 2nd-L, 3rd-L), the first torsional (1st-T) and the first coupled longitudinal-torsional (1st-L-T) modes. The polar plot representation of a mode shape provides information on the degree of non-classical (or non-proportional) damping (Veletsos and Ventura 1986) characteristics of that mode. If all components of a mode shape (each component being represented by a vector in a polar plot) are collinear, that vibration mode is classically damped.

The more scattered the mode shape components are in the complex plane, the more the system is non-classically (non-proportionally) damped in that mode. However, measurement noise (low signal-to-noise ratio), estimation errors, and modeling errors can also cause a truly classically damped vibration mode to be identified as non-classically damped. From Figure 4, it is observed that the first longitudinal and first torsional modes at damage state S2 are identified as perfectly classically damped. Some degree of non-proportional damping is identified for the other modes (2^{nd}-L , 3^{rd}-L , and 1^{st}-L-T).

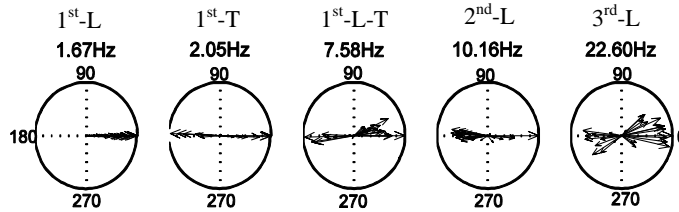


Fig. 4 Polar plot representation of complex-valued mode shapes of the building at damage state S2 obtained using SSI-DATA based on ambient vibration data

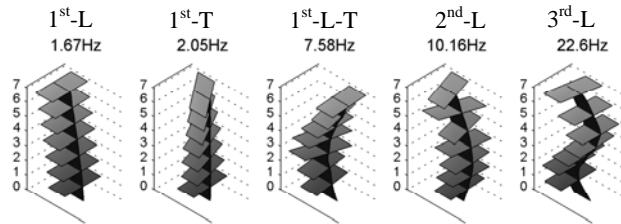


Fig. 5 Vibration mode shapes of the building at damage state S2 obtained using SSI-DATA based on ambient vibration data

The natural frequencies and damping ratios of the five most significantly excited modes identified based on ambient vibration acceleration data are given in Table 2 for all damage states considered and the three output-only system identification methods used (MNE_xT-ERA, SSI-DATA, EFDD). From Table 2, it is observed that: (1) the natural frequencies identified using different methods are in good agreement at each damage state, while the identified damping ratios display larger variability across the different system identification methods. (2) The identified natural frequencies of the longitudinal modes (1^{st}-L , 2^{nd}-L , 3^{rd}-L) decrease consistently with increasing level of damage, except from damage states S3.1 to S3.2, when the steel braces were modified (stiffened), while the identified damping ratios do not exhibit a clear trend as a function of structural damage. (3) The first torsional vibration mode (1^{st}-T) could only be identified at damage states S2, S3.1 and S3.2. (4) The identified damping ratios are in a reasonable range (0-

5%). (5) The modal damping ratios identified using EFDD are systematically lower than their counterparts identified using the other two methods. This can be due to the fact that in the application of EFDD, a high Modal Assurance Criterion (MAC) value is used to decompose the noisy CSD functions into narrow peak (low-damped) SDOF CSD functions.

Table 5. MAC values between corresponding mode shapes identified using different methods based on ambient vibration test data

State / Test No.	System ID Method	1 st -L mode	1 st -T mode	1 st -L-T mode	2 nd -L mode	3 rd -L mode
S0 / Test 39	MNExT & SSI*	0.99	-	0.26	0.86	0.7
	MNExT & EFDD	0.99	-	0.46	0.49	0.74
	SSI & EFDD	1	-	0.82	0.77	0.97
S1 / Test 41	MNExT & SSI	0.91	-	0.78	0.89	0.79
	MNExT & EFDD	0.97	-	0.84	0.89	0.88
	SSI & EFDD	0.79	-	0.84	0.98	0.89
S2 / Test 46	MNExT & SSI	1	0.98	0.98	0.56	0.95
	MNExT & EFDD	1	0.98	0.96	0.43	0.96
	SSI & EFDD	1	1	0.98	0.97	0.95
S3.1 / Test 49	MNExT & SSI	0.99	-	0.92	0.39	0.93
	MNExT & EFDD	1	-	0.78	0.49	0.96
	SSI & EFDD	0.99	-	0.92	0.96	0.98
S3.2 / Test 61	MNExT & SSI	1	0.97	-	1	0.97
	MNExT & EFDD	1	0.98	-	1	0.98
	SSI & EFDD	1	0.98	-	1	0.99
S4 / Test 64	MNExT & SSI	1	-	-	0.99	0.96
	MNExT & EFDD	1	-	-	0.99	0.98
	SSI & EFDD	1	-	-	1	0.98

* SSI denotes SSI-DATA and MNExT denotes MNExT-ERA

Modal Assurance Criterion (MAC) values (Allemang and Brown 1982) were computed to compare the corresponding complex-valued mode shapes identified using the three output-only system identification methods considered and are reported in Table 5. The high MAC values obtained in most cases (each case being defined by a vibration mode, a pair of system identification methods and a damage state) indicate a good agreement in general between the mode shapes identified using different methods. From Table 5, it is also observed that the MAC values between corresponding mode shapes identified using SSI-DATA & EFDD are in general the highest among the three combinations of system identification methods (i.e., MNExT-ERA

& SSI-DATA, MNExT-ERA & EFDD, SSI-DATA & EFDD). The low MAC values between mode shapes identified using MNExT-ERA & SSI-DATA and MNExT-ERA & EFDD for the 1st-L-T mode at damage state S0 and 2nd-L mode at damage states S2 and S3.1 imply that these mode shapes identified using MNExT-ERA are the least accurate among the three output-only methods considered. This could be due to the fact that in the application of MNExT-ERA, if the selected reference channels are close to modal nodes of a vibration mode, the estimation uncertainty of that mode is relatively large (He et al. 2009).

Modal Parameters Identified Based on 0.03g RMS White Noise Base Excitation Test Data

The modal parameters identified based on acceleration data from 0.03g RMS white noise base excitation tests are presented and discussed in this section. Figure 6 shows in polar plots the complex-valued mode shapes of the five most significant modes of the building identified using MNExT-ERA based on data from Test 39 (damage state S0). The five most significant vibration modes identified in this case consist of the first three longitudinal (1st-L, 2nd-L, 3rd-L), the first torsional (1st-T), and the first coupled longitudinal-torsional (1st-L-T) modes. From Figure 6, it is observed that the first longitudinal (1st-L) vibration mode is identified as nearly perfectly classically damped, while the other identified modes (1st-T, 1st-L-T, 2nd-L, 3rd-L) display some non-classical damping characteristics.

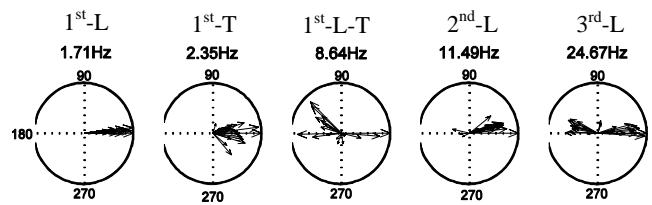


Fig. 6 Polar plot representation of complex-valued mode shapes of the building at damage state S0 obtained using MNExT-ERA based on white noise base excitation test data

Table 3 reports the natural frequencies and damping ratios of the five most significantly excited vibration modes identified using the six system identification methods based on acceleration data from the 0.03g RMS white noise base excitation tests at all damage states considered. From Table 3, it is observed that: (1) the natural frequencies identified using different methods are reasonably consistent at each damage state, while the identified damping ratios exhibit much larger variability. It appears that when a mode is not significantly excited, its modal damping

identified using EFDD is consistently very low compared to other methods. (2) Some vibration modes (especially the first torsional mode) could not be identified by each of the system identification methods. (3) The natural frequencies of all identified vibration modes decrease consistently with increasing level of structural damage, except from damage state S3.1 to S3.2, when the steel braces were modified (stiffened), while the identified damping ratios do not exhibit a clear trend as a function of damage. (4) At each damage state, the identified modal parameters of the first longitudinal mode (1st-L) appear to be the least sensitive to the identification method used, which could be due to the predominant contribution of this mode to the total response.

Table 6 reports the MAC values calculated between corresponding complex-valued mode shapes identified using the three output-only system identification methods (i.e., MNEXT-ERA & SSI-DATA, MNEXT-ERA & EFDD, SSI-DATA & EFDD), the three input-output system identification methods (i.e., DSI & OKID-ERA, DSI & GRA, OKID-ERA & GRA), and also between corresponding mode shapes identified using an output-only and an input-output system identification method (SSI-DATA & GRA). From the results in Table 6, it is observed that: (1) the MAC values calculated for the 1st-L mode shape identified using different methods are very close to unity for all damage states considered (i.e., low level of estimation uncertainty), implying that these identified mode shapes are probably close to the actual 1st-L mode shape of the structure. (2) Lower MAC values obtained for the 1st-L-T mode shape indicate its larger estimation uncertainty compared to other modes. (3) In general, the MAC values calculated across output-only methods are higher than those calculated across input-output methods. It should be noted that the output-only methods perform very well (are very accurate) when the hypothesis based on which they are developed are satisfied (i.e., when the input excitation is a white noise sequence). (4) The MAC values between corresponding mode shapes identified using SSI-DATA (output-only method) and GRA (input-output method) are in general high indicating that the corresponding mode shapes are in good agreement, especially for the three longitudinal mode shapes (i.e., 1st-L, 2nd-L, 3rd-L).

Table 6. MAC values between corresponding mode shapes identified using different methods based on 0.03g RMS white noise base excitation test data

State / Test No.	System ID Method	1 st -L mode	1 st -T mode	1 st -L-T mode	2 nd -L mode	3 rd -L mode
S0 / Test 39	MNExT & SSI	1	-	0.9	0.96	0.99
	MNExT & EFDD	0.99	-	0.82	0.94	0.97
	SSI & EFDD	1	-	0.82	0.97	0.99
	DSI & OKID	1	-	0.58	0.65	0.92
	DSI & GRA	1	-	0.66	0.24	0.8
	OKID & GRA	1	-	0.76	0.71	0.94
	SSI & GRA	1	-	0.7	0.95	0.98
S1 / Test 41	MNExT & SSI	1	0.96	0.51	0.99	0.99
	MNExT & EFDD	1	-	0.75	0.96	0.99
	SSI & EFDD	1	-	0.49	0.99	1
	DSI & OKID	1	-	-	0.54	0.83
	DSI & GRA	1	-	0.49	0.39	0.88
	OKID & GRA	1	-	-	0.9	0.56
	SSI & GRA	1	-	0.3	0.99	0.99
S2 / Test 46	MNExT & SSI	1	-	0.76	0.97	0.67
	MNExT & EFDD	1	-	0.82	0.98	0.86
	SSI & EFDD	1	-	0.81	0.99	0.87
	DSI & OKID	1	-	0.24	0.2	0.91
	DSI & GRA	1	-	0.59	0.22	0.64
	OKID & GRA	1	-	0.44	0.89	0.72
	SSI & GRA	1	-	0.73	0.99	0.98
S3.1 / Test 49	MNExT & SSI	1	-	0.54	0.97	0.73
	MNExT & EFDD	1	-	0.42	0.98	0.76
	SSI & EFDD	1	-	0.8	0.99	0.75
	DSI & OKID	1	-	0.48	-	0.88
	DSI & GRA	1	-	0.65	-	0.86
	OKID & GRA	1	-	0.84	0.78	0.94
	SSI & GRA	1	-	0.74	0.95	0.9
S3.2 / Test 61	MNExT & SSI	1	0.7	-	0.94	0.99
	MNExT & EFDD	1	-	-	0.85	0.89
	SSI & EFDD	1	-	-	0.84	0.9
	DSI & OKID	1	-	-	-	0.91
	DSI & GRA	1	-	-	-	0.9
	OKID & GRA	1	-	-	-	0.97
	SSI & GRA	1	-	-	0.72	0.98
S4 / Test 64	MNExT & SSI	1	-	-	0.99	0.51
	MNExT & EFDD	1	-	-	0.96	0.58
	SSI & EFDD	1	-	-	0.96	0.94
	DSI & OKID	1	-	-	0.97	0.68
	DSI & GRA	1	-	-	0.94	0.91
	OKID & GRA	1	-	-	0.93	0.77
	SSI & GRA	1	-	-	0.97	0.73

Modal Parameters Identified Based on 0.05g RMS White Noise Base Excitation Test Data

In order to investigate the effect of excitation amplitude (and therefore level of response nonlinearity) on the identified effective modal parameters, the modal parameters of the first three longitudinal vibration modes are also identified based on acceleration data from 0.05g RMS white noise base excitation tests and are presented and discussed in this section. Table 4 reports the natural frequencies and damping ratios of the three longitudinal vibration modes identified based on acceleration data from 0.05g RMS white noise base excitation tests at damage states S1, S2, S3.1 and S4. From Table 4, it is observed that: (1) the natural frequencies identified using different methods are reasonably consistent at each damage state, while the identified damping ratios exhibit much larger variability. (2) The identified natural frequencies of all identified vibration modes decrease with increasing level of structural damage, while the identified damping ratios do not exhibit a clear trend as a function of damage.

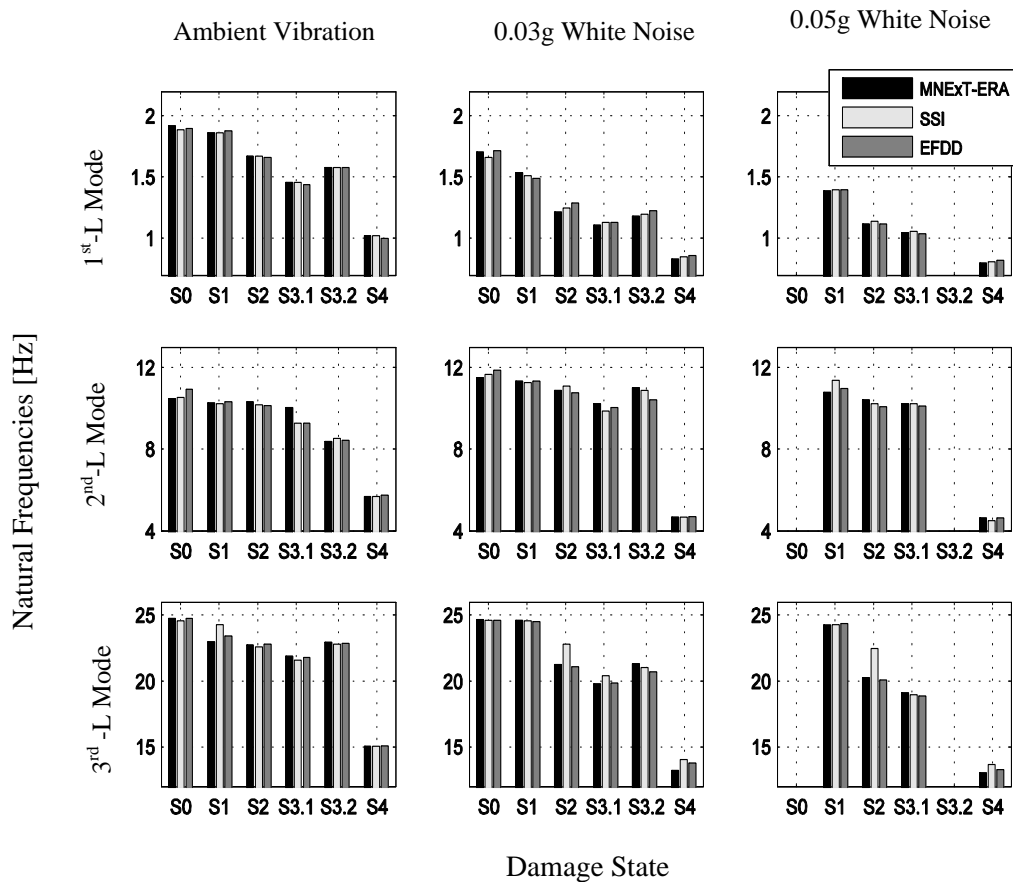


Fig. 7 Natural frequencies of the first three longitudinal modes identified based on ambient and white noise base excitation (0.03g, and 0.05g RMS) test data using different methods

Figures 7 and 8 show the natural frequencies and damping ratios of the three longitudinal modes, respectively, identified using the three output-only methods based on ambient vibration, 0.03g, and 0.05g RMS white noise base excitation test data. By comparing the modal parameters identified at different levels of excitation (i.e., ambient, 0.03g, and 0.05g RMS white noise base excitation), it is observed that: (1) the (effective) natural frequencies of the three longitudinal vibration modes identified based on higher amplitude response data are in general lower than their counterparts identified based on lower amplitude response data at all damage states considered. The difference is more significant for the first longitudinal vibration mode (an average of 20% reduction in the identified first modal frequencies from ambient vibration data to 0.03g white noise base excitation data and 26% reduction from ambient vibration data to 0.05g white noise base excitation data). This is most likely due to the fact that the test structure is nonlinear (even at the relatively low levels of excitation considered in this system identification study) with effective modal parameters depending strongly on the intensity of the excitation and therefore of the structural response, reflecting the fact that concrete cracks open wider with increasing intensity of the excitation. It is also worth noting that the first natural frequency of the uncracked structure identified based on ambient vibration data (2.23Hz obtained using peak picking method) is significantly higher than its counterpart for the cracked structure at the undamaged state S0 (average of 1.90Hz over the three output-only methods). (2) In general, higher modal damping ratios are identified for the three longitudinal vibration modes during the higher amplitude (0.05g RMS) base excitation tests. There is an average relative increase of 110% in damping ratios of the three longitudinal modes from ambient vibration data to 0.03g white noise base excitation data and 230% from ambient vibration data to 0.05g white noise base excitation data. This reflects the additional hysteretic damping at higher level of response nonlinearity, which is identified as equivalent linear viscous damping by the linear system identification methods used in this study.

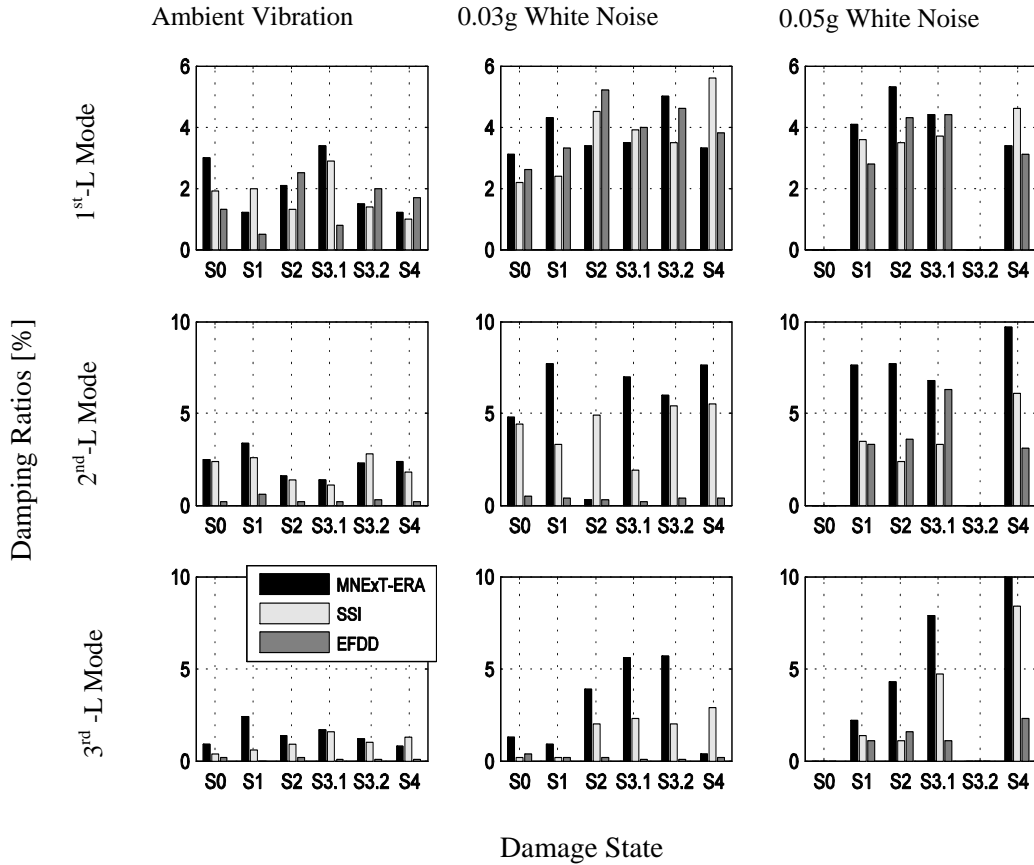


Fig. 8 Damping ratios of the first three longitudinal modes identified based on ambient and white noise base excitation (0.03g, and 0.05g RMS) test data using different methods

SUMMARY AND CONCLUSIONS

A full-scale seven-story reinforced concrete building slice was tested on the UCSD-NEES shake table in the period October 2005 - January 2006. The shake table tests were designed to damage the building progressively through several historical earthquake ground motions reproduced on the shake table. At several levels of damage, ambient vibration tests and low amplitude white noise base excitation tests were applied to the building which responded as a quasi-linear system with dynamic parameters evolving as a function of structural damage. Six different state-of-the-art system identification methods including three output-only and three input-output methods were used to estimate the modal parameters (natural frequencies, damping ratios, and mode shapes) of the building in its undamaged (baseline) and various damage states

based on the response of the building to ambient as well as white noise base excitations measured using 28 DC-coupled accelerometers.

From the results of this system identification study, it is observed that: (1) the natural frequencies identified using different methods are reasonably consistent at each damage state, while the identified damping ratios exhibit much larger variability across system identification methods. (2) The identified natural frequencies of the three longitudinal vibration modes decrease with increasing level of damage except from damage state S3.1 to S3.2, when the steel braces were stiffened. The identified modal damping ratios do not follow a clear trend as a function of structural damage. (3) At each damage state, the identified modal parameters of the first longitudinal mode appear to be the least sensitive to the identification method used, which is most likely due to the predominant contribution of this mode to the total response. (4) The (effective) natural frequencies of the three longitudinal vibration modes identified based on higher amplitude response data are in general lower than their counterparts identified based on lower amplitude response data at all damage states considered, especially for the first longitudinal vibration mode. This is most likely due to the fact that the test structure is nonlinear (even at the relatively low levels of excitation considered in this system identification study) with effective modal parameters depending strongly on the amplitude of the excitation and therefore of the structural response. (5) In general, higher modal damping ratios are identified for the three longitudinal vibration modes during the higher amplitude base excitation tests. This is due to the fact that the additional hysteretic damping at higher level of response nonlinearity is identified as equivalent viscous damping by the linear system identification methods used here. It should be emphasized that these “inflated” identified equivalent viscous damping ratios are not to be used to represent the viscous damping component in a nonlinear FE model of a structure that explicitly accounts for the nonlinear material behavior. Panagiotou (2008) showed that the viscous damping ratios required to best “reproduce” computationally, using nonlinear dynamic time history analysis, the experimentally measured response are significantly lower than those identified in this study. Also in this study, it was found that the modal parameters (natural frequencies and mode shapes) computed from a linear elastic finite element model of the building structure developed based on gross section properties are in good agreement with their experimental counterparts identified based on ambient vibration data recorded from the uncracked structure (Moaveni 2007). The modal parameters identified at various damage states

in this study provide the input for damage identification of this seven-story building using a sensitivity-based finite element model updating strategy (Moaveni et al. 2009).

The above presented linear system identification study performed on a densely instrumented full-scale reinforced concrete building specimen raises the need to apply to this type of testbed structures: (1) probabilistic system identification methods (e.g., Bayesian system identification) in order to treat consistently the quantification and propagation of the various sources of aleatory and epistemic (modeling) uncertainty affecting the system identification results, and (2) nonlinear system identification methods (e.g., nonlinear finite element model updating) in order to capture the various sources (e.g., material, geometric, contact) of nonlinearity affecting the structural response and in order to use the dynamic output and possibly input data of the damaging event (e.g., earthquake) in the identification process.

ACKNOWLEDGEMENTS

Partial supports for this research from Lawrence Livermore National Laboratory with Dr. David McCallen as Program Leader and from Englekirk Center Board of Advisors are gratefully acknowledged. The authors would also like to thank Dr. Marios Panagiotou and Dr. Ozgur Ozcelik as well as the technical staff at the Englekirk Structural Engineering Center for their help in collecting the test data. Any opinions, findings, and conclusions or recommendations expressed in this material are those of the authors and do not necessarily reflect those of the sponsors.

REFERENCES

- Allemang, R. J., and Brown, D. L. (1982). "A correlation coefficient for modal vector analysis." *Proc. of 1st International Modal Analysis Conference, IMAC I*, Bethel, Connecticut.
- Brincker, R., Ventura, C., and Andersen, P. (2001). "Damping estimation by frequency domain decomposition." *Proc. of International Modal Analysis Conference, IMAC XIX*, Kissimmee, USA.
- De Callafon, R. A., Moaveni, B., Conte, J. P., He, X., and Udd, E. (2008). "General realization algorithm for modal identification of linear dynamic systems." *Journal of Engineering Mechanics*, ASCE, 134(9), 712-722.
- Doebling, S. W., Farrar, C. R., Prime, M. B., and Shevitz, D. W. (1996). *Damage identification in structures and mechanical systems based on changes in their vibration characteristics: a detailed literature survey*. Los Alamos National Laboratory Report, LA-13070-MS, Los Alamos, New Mexico, USA.
- Doebling, S. W., Farrar, C. R., and Prime, M. B. (1998). "A summary review of vibration-based damage identification methods." *The Shock and Vibration Digest*, 30(2), 99-105.
- He, X., Moaveni, B., Conte, J. P., Elgamal A., and Masri, S. F. (2009). "System identification of Alfred Zampa Memorial Bridge using dynamic field test data." *Journal of Structural Engineering*, ASCE, 135(1), 54-66.
- James, G. H., Carne, T. G., and Lauffer, J. P. (1993). *The natural excitation technique for modal parameters extraction from operating wind turbines*. Sandia National Laboratories Report, SAND92-1666, UC-261, Sandia, New Mexico, USA.
- Juang, J. N., and Pappa, R. S. (1985). "An eigensystem realization algorithm for model parameter identification and model reduction." *J. Guidance Control Dyn.*, 8(5), 620-627.
- Lus, H., Betti, R., and Longman, R. W. (2002). "Obtaining refined first order predictive models of linear structural systems." *Earthquake Eng. Struct. Dyn.*, 31(7), 1413-1440.
- Moaveni B. (2007). *System and damage identification of civil structures*. Ph.D. Dissertation, Department of Structural Engineering, University of California, San Diego, CA.

- Moaveni, B., Barbosa, A. R., Conte, J. P., and Hemez, F. M. (2007). "Uncertainty analysis of modal parameters obtained from three system identification methods." *Proc. of International Conference on Modal Analysis (IMAC-XXV)*, Orlando, USA.
- Moaveni, B., He, X., Conte, J. P., and Restrepo, J. I. (2010). "Damage identification study of a seven-story full-scale building slice tested on the UCSD-NEES shake table." *Structural Safety*, 32(5), 347-356.
- Ozcelik, O. (2008). *A Mechanics-based virtual model of NEES-UCSD shake table: theoretical development and experimental validation*. Ph.D. Dissertation, Department of Structural Engineering, University of California, San Diego, CA.
- Panagiotou, M. (2008). *Seismic design, testing and analysis of reinforced concrete wall buildings*. Ph.D. Thesis, Department of Structural Engineering, University of California, San Diego, CA.
- Panagiotou M, and Restrepo J. I. (2009a). "A Displacement-based method of analysis for regular reinforced concrete wall buildings: Application to a full-scale 7-story building slice tested at UC San Diego." *Journal of Structural Engineering*, ASCE, under review.
- Panagiotou M., Restrepo J. I., and Conte J. P. (2009b). "Shake table test of a full-scale 7-story building slice - Phase I: rectangular wall." *Journal of Structural Engineering*, ASCE, under review.
- Phan, M., Horta, L. G., Juang, J.-N., and Longman, R. W. (1992). *Identification of linear systems by an asymptotically stable observer*. NASA Tech. Paper, 3164.
- Sohn, H., Farrar, C. R., Hemez, F. M., Shunk, D. D., Stinemates, D. W., and Nadler, B. R. (2003). *A review of structural health monitoring literature: 1996-2001*. Los Alamos National Laboratory Report, LA-13976-MS, Los Alamos, New Mexico, USA.
- Van Overschee, P., and de Moore, B. (1996). *Subspace identification for linear systems*, Kluwer Academic Publishers, Massachusetts, USA.
- Veletsos, A. S., and Ventura, C. E. (1986). "Modal analysis of non-classically damped linear systems." *Earthq. Engng. Struct. Dyn.*, 14(2), 217-243.